Multiphoton detachment of negative ions in an intense radiation field

L. A. Collins and A. L. Merts
Group T-4, Los Alamos National Laboratory, Los Alamos, New Mexico 87545
(Received 16 October 1991)

We have applied a momentum-space method to the solution of the three-dimensional time-dependent Schrödinger equation for electron detachment from a model negative ion, in particular H^-. We have studied such phenomena as excess-photon detachment and threshold effects. For selected cases, we obtain excellent agreement with the Floquet calculations. We also present results in regimes of strong interest to experimental efforts.

PACS number(s): 32.80.Fb, 32.80.Wr

I. INTRODUCTION

The negative ion of hydrogen provides an excellent opportunity to study intense-field effects at modest intensities. Since these effects depend more upon the relative strengths of the binding and laser fields, they manifest themselves in a weakly bound system as H^- for an intensity regime beginning at only about 10^{11} W/cm^2 or 0.0017 a.u. of the electric field. The regime abounds with many new and interesting phenomena. One mechanism of particular interest is excess-photon detachment (EPD), the analog of above-threshold ionization (ATI) for neutral atoms. For a laser of frequency ω incident upon an ion, we observe a series of peaks in the electron distribution that are separated by $\hbar\omega$ and positioned at and above the energy corresponding to the minimum number of photons needed to break the atomic bond. The simplicity of the H^- system has attracted much experimental [1–5] and theoretical [6–24] attention. While no direct observation of EPD exists for H^-, the phenomenon has been seen in F^- [3], Cl^- [4], and Au^- [5]. Not surprisingly, the earliest applications of the Keldysh-style formulations [6–8] addressed the detachment from H^-. In addition, more sophisticated approaches [9–18] have been employed from scattering-theoretic to Floquet analysis. To date, the time-independent Floquet method [9–11] provides the most detailed treatment of this system. We have applied our time-dependent (TD) momentum-space formulation [18] to a simple three-dimensional (3D) one-electron model of the H^- system and have investigated the intense-field regime for several frequencies, especially concentrating on the EPD mechanism and threshold behavior. Our results complement the Floquet analysis and provide a TD picture of the detachment process. Since a series of excellent comprehensive reviews [19–27] amply covers all aspects of intense-field interactions with atomic species, we focus our attention solely on the behavior of model negative ions in this regime.

II. FORMULATION

Since we have presented a detailed formulation elsewhere [18], we give only a brief exposition of the technique employed to solve the three-dimensional time-dependent Schrödinger equation

$$[-\tfrac{1}{2}\nabla^2+V_a(\mathbf{r})+V_e(\mathbf{r}|t)]\psi(\mathbf{r}|t)=iD_t\psi(\mathbf{r}|t)\ , \tag{1}$$

which represents a single electron subject to an atomic potential $V_a(\mathbf{r})$ in the presence of an time-varying potential $V_e(\mathbf{r}|t)$ with D_t given by $\partial/\partial t$ and ∇^2, the usual Laplacian. Since we seek to examine the interaction of an electric field with the atom, we invoke the dipole approximation and write the TD potential in the $\mathbf{E}\cdot\mathbf{r}$ gauge as

$$V_e(\mathbf{r}|t)=\mathbf{E}(\mathbf{r}|t)\cdot\mathbf{r}\ ,$$

with the electric field taken in a particularly simple form,

$$\mathbf{E}(\mathbf{r}|t)=f(t)E_0\sin(\omega t)\hat{\mathbf{e}}\ . \tag{2}$$

With this choice, the unit vector $\hat{\mathbf{e}}$ represents the orientation of an oscillating electric field with frequency ω and period $T\ (=2\pi/\omega)$; the function $f(t)$ allows the field to depart from purely periodic behavior. We have an initial-value problem such that at time $t=0$ the wave function $\psi(\mathbf{r}|0)$ assumes a known functional form. From this basic structure of the TD Schrödinger equation, we turn to a description of its solution.

We construct a total system wave function by expanding in terms of a complete set of basis states in momentum ($\mathbf{k}$) space as

$$\psi(\mathbf{r}|t)=\int a(\mathbf{k}|t)\phi_{\mathbf{k}}(\mathbf{r}|t)d\mathbf{k}\ . \tag{3}$$

We select our basis states to solve the Schrödinger equation

$$[-\tfrac{1}{2}\nabla^2+V_e(\mathbf{r}|t)]\phi_{\mathbf{k}}(\mathbf{r}|t)=iD_t\phi_{\mathbf{k}}(\mathbf{r}|t), \tag{4}$$

which resembles Eq. (1) without the atomic interaction. From our choice of field in Eq. (2), we immediately identify these solutions as the familiar Volkov states [28], which obey the normalization condition

$$\int\phi_{\mathbf{k}'}(\mathbf{r}|t)^*\phi_{\mathbf{k}}(\mathbf{r}|t)d\mathbf{r}=\delta(\mathbf{k}'-\mathbf{k})\ . \tag{5}$$

By substituting Eq. (3) into Eq. (1), multiplying through by a representative state $\phi_{\mathbf{k}'}(\mathbf{r}|t)^*$, and integrating over the spatial coordinates, we convert the Schrödinger equa-

tion into a set of first-order (FO) coupled temporal equations of the form

$$D_t a(\mathbf{k}'|t) = -i \int M(\mathbf{k}',\mathbf{k}|t) a(\mathbf{k}|t) d\mathbf{k} , \tag{6}$$

with the matrix elements given by

$$M(\mathbf{k}',\mathbf{k}|t) = \int \phi_{\mathbf{k}'}(\mathbf{r}|t)^* V_a(\mathbf{r}) \phi_{\mathbf{k}}(\mathbf{r}|t) d\mathbf{r} . \tag{7}$$

An interesting point arises concerning the choice of gauge. The matrix elements in Eq. (7) are exactly the same in the $\mathbf{E}\cdot\mathbf{r}$ and the $\mathbf{P}\cdot\mathbf{A}$ gauges, since the respective Volkov solutions differ only in spatial parts independent of $\mathbf{k}$. We limit our discussion to linearly polarized light and choose the cylindrical coordinates (z,ρ,φ) as providing the most convenient representation. For a spherically symmetric atomic potential, we further simplify by expanding the system wave function in terms of states of the angular coordinate φ as

$$\psi(\mathbf{r}|t) = \sum_m \phi_m(\varphi) \int a_{\bar{\mathbf{k}}m}(t) \phi_{\bar{\mathbf{k}}m}(\mathbf{r}|t) d\bar{\mathbf{k}} , \tag{8}$$

where

$$\phi_m(\varphi) = (2\pi)^{-1/2} \exp(im\varphi) , \tag{9}$$

m is an integer, and the vector $\bar{\mathbf{k}}$ represents the two momenta (κ,q) analogous to the cylindrical spatial variables (z,ρ). Substituting this expression into Eq. (6), multiplying through by a representative function $\phi_{m'}(\varphi)^*$, and integrating over the angular coordinate, we obtain a set of two-dimensional FO temporal equations, block diagonal in the azimuthal quantum number m. In some cases, we prefer to employ the polar variables (K,θ) defined as $K=\kappa^2+q^2$ and $\tan\theta=\kappa/q$. In practice, we designate a discrete set of momentum-space $\bar{\mathbf{k}}$ values and convert the integrals to sums and the temporal equations to the finite matrix representation

$$\dot{\mathbf{a}}(t) = -i\mathbf{M}(t)\mathbf{a}(t) , \tag{10}$$

where $[\mathbf{a}(t)]_\alpha = a_\alpha(t)$ and $[\mathbf{M}(t)]_{\alpha\alpha'} = M_{\alpha\alpha'}(t) w_{\alpha\alpha'}$ in terms of an index $\alpha \equiv (K,\theta)$. The matrix elements $M_{\alpha\alpha'}(t)$ are defined by Eq. (7); the weights, employed to make the 2D integral in Eq. (6) discrete, are given by $w_{\alpha\alpha'}$; and the superscript "dot" represents a time differentiation. We have tested several techniques for propagating this FO temporal matrix equation, including second-order differences (SOD) [27] and Gear [29] techniques. In addition, we extended the Lanczos reduction technique of Park and Light [30] to a TD Hamiltonian. The most general choice of weights in Eq. (6) yields a nonsymmetric propagation matrix. We therefore employed reduction to the upper-Hessenberg rather than to the tridiagonal form. If we select the weights as positive definite, then a transformation brings the temporal matrix equations into symmetric representation [18]. We find that the SOD method functions as well as the others and requires less storage. For this reason, we have employed the SOD procedure as our principal propagator but have assiduously checked its results with the more sophisticated schemes.

We must now devise a model to describe the negative ion of hydrogen. Following Shakeshaft and Tang [9], we treat H^- as a one-electron system described by the potential.

$$V_a(r) = -V_0 \exp(-\beta r)/r , \tag{11}$$

where $V_0 = 1.1$ and $\beta = 1$. The parameters of the Yukawa potential are selected to give a bound wave function $\phi_0(\mathbf{r}|t)$ in reasonably good agreement with its full two-electron counterpart. We use this wave function as the initial condition for our temporal propagation. This potential supports a single bound state at an energy of $\varepsilon_b = -0.027\,565\,4$ hartree (0.75 eV), the correct binding energy of H^-. The question immediately arises as to the degree to which such a model can represent the actual two-electron system. Estimates of the many-electron effects indicate that for the intensity and frequency range under consideration, this simple model gives reasonably reliable results [10].

Our principal interest rests with the detachment rates and energy distributions of the freed electron. Since our model has but one bound level, we define a detachment rate in terms of the depletion of this state. The probability that the system remains in the ground state at time t is given by the simple projection

$$P_b(t) = \left| \int \phi_0(\mathbf{r}|t)^* \psi(\mathbf{r}|t) d\mathbf{r} \right|^2 . \tag{12}$$

We in turn define an effective rate $W(t)$ of depletion of this state by the relationship

$$P_b(t) \equiv \exp[-W(t)t] . \tag{13}$$

Of course, the rate at which the bound state is depleted equals the rate at which the H^- detaches so that W also represents a detachment rate. In many situations, the effective rate oscillates in time about a single constant value. For this circumstance, we also define a time-averaged rate over a cycle W_a, which unambiguously characterizes the detachment process after the initial transient phase. We determine the electron-energy distribution from a projection onto the momentum basis states. Thus, the probability at time t of finding the electron with momentum $\bar{\mathbf{k}}$ is given by $|a_{\bar{\mathbf{k}}}(t)|^2$. Since this quantity is two dimensional, we seek a more appropriate form for display by expanding in terms of associate Legendre polynomials $\otimes_{lm}(\theta)$ in the polar angle θ as

$$a_{\bar{\mathbf{k}}m}(t) = \sum_l A_{lm}(K|t) \otimes_{lm}(\theta) . \tag{14}$$

We make one final adjustment by employing the projection function $P_{lm}(t)$ defined by

$$P_{lm}(K|t) \equiv K^2 |A_{lm}(K|t)|^2 \tag{15}$$

such that

$$\sum_l \int P_{lm}(K|t) dK = 1 . \tag{16}$$

This final expression simply implies that the system wave function must have unit probability of being somewhere in space—the analog of the spatial integral of the square modulus of $\psi(\mathbf{r}|t)$. The $P_{lm}(K|t)$ coefficients, which

represent the probability of finding the detached electron with a particular energy $K^2/2$ with a certain orbital angular momentum l, will give a description of the EPD structure, both the positions and the angular composition of its peaks. Finally, by summing over the angular components, we obtain a total probability $P_m(K|t)$, which would be the most likely feature observed experimentally. The probabilities discussed above involve projections onto the Volkov states and therefore represent an electron free of the atomic potential but remaining in the oscillating electric field. However, if we perform the calculations at an integer multiple of the period T, then the resulting probabilities correspond to projections on a simple plane wave, independent of the potential and the radiation field. This situation corresponds to most experimental arrangements in which the detached electrons are detected outside of the laser pulse. The manner in which the electron exits the field also characterizes the structure of the EPD peaks. In an earlier study [18], we investigated the effects of the temporal and spatial ramping of the oscillating electric field on the electron-energy distribution. For all examples in this article, we report EPD electron spectra for a field that temporally switches off long before the electron can exit the spatial extent of the pulse. Our EPD graphs best resemble an experiment with short pulses and low-energy detached electrons, although other representations can be constructed from the TD propagated wave function.

We have made several improvements in the original implementation. We had determined the matrix elements in Eq. (7) by direct integration. However, we found that the oscillating integrands encountered in such momentum-space formulations were difficult to converge in this manner. We therefore expanded the atomic potential in a set of floating Gaussian or B spline functions. The spatial integration over the Gaussians and oscillating functions could in most cases be performed analytically with the full integral found by summing over the expansion terms. This procedure has proven to be both more accurate and more efficient. We also employ the technique for the representation of the initial wave function in the projection integrations. Finally, we have found that the polar representation is generally more compact than the rectangular and will usually place our momentum-space meshes in terms of K and θ.

In closing this section, we observe that the method to date has been applied to short-ranged atomic potentials and has demonstrated the general behavior of EPD (ATI) peaks and ionization rates characteristic of many experiments. In addition, the method correctly reproduces the perturbation limit for low intensities. For the Yukawa potential, we have obtained excellent agreement with a Floquet solution [31] of the TD Schrödinger equation in the Kramers-Henneberger gauge for ionization rates. The Floquet analysis in turn produces results for H in very good agreement with other TD theoretical methods, which have been extensively compared with observed phenomena. This correlation lends considerable validity to the basic momentum-space approach as applied to negative ions. With the basic techniques expounded, we embark upon a description of the results.

III. RESULTS AND DISCUSSION

We describe the detachment of H^- for different frequency and intensity environments. Our interest naturally centers on those regimes most open to experimental investigation. We begin by demonstrating the efficacy of the technique by reproducing the perturbation limit. Having ascertained the quality of the method, we explore detachment processes requiring one and more photons. Before launching into a detailed discussion, we describe several common features of the calculations. First, since the system has only one bound state with symmetry $m=0$, we need only consider this one symmetry block in determining the detachment parameters. This simplification greatly reduces the computational effort. Second, we employ the (K,θ) variables to label the expansion coefficients and matrix elements. We divide the K-space regime into a series of N zones, each with a prescribed number of points. The nomenclature for this mesh takes the form $[n_1,n_2,\ldots,n_N/0,K_1,K_2,\ldots,K_N]$. The first entry gives the number of points in each zone n_i, while the second designates the boundaries. For example, zone 2 has n_2 points and extends from K_1 to K_2. The total number N_K of mesh points in the K variable is simply the sum of the individual zone counts. Our angular mesh spans a single zone from 0 to π with N_θ points. Therefore, the order of the matrix that must be temporally propagated is $N_K N_\theta$. For both variables, we usually select a Gauss-Legendre quadrature to determine the weights and the distribution of points in the integral evaluation in Eq. (6), although Simpson's rule has also been applied. Third, we have found that a temporal step size of $\Delta t = T/7500$ gives accurate wave-packet propagation in the SOD method. In most cases, we turn the field on by the simple relation in Eq. (2). However, we have employed a linear ramp of several periods but have found little difference with the instantaneous result. With these special features in mind, we can begin our exposition of the calculations.

A. One-photon detachment

As an example, we treat the detachment of an electron from H^- by the absorption of a single photon ($\omega > \epsilon_b$).

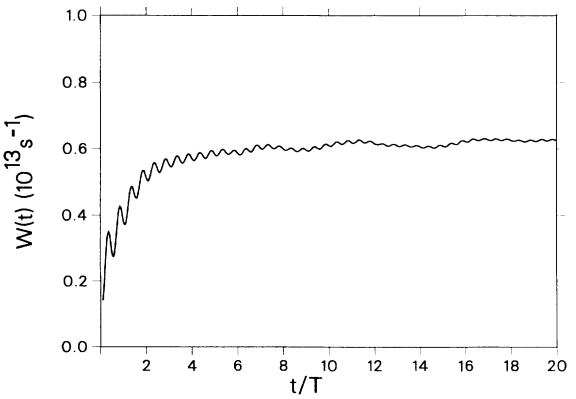

FIG. 1. Effective detachment rate $W(t)$ as a function of time for $\omega=0.043$ hartree (1.17 eV) and an intensity of $I=5\times10^{10}$ W/cm^2 ($E_0=0.001\,19$ a.u.).

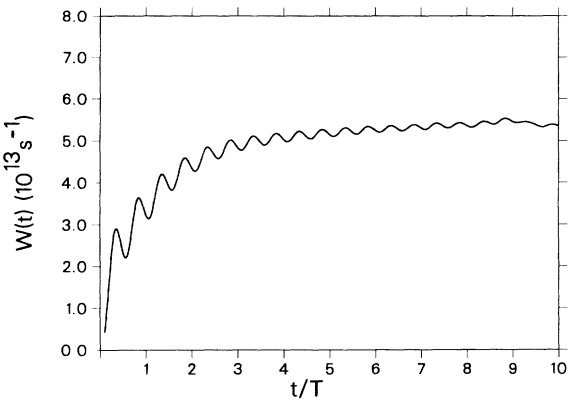

FIG. 2. Same as Fig. 1 but for $I=5\times10^{11}$ W/cm^2 (0.003 78 a.u.).

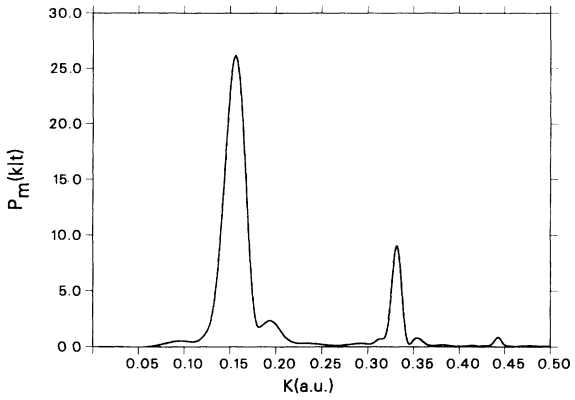

FIG. 4. Same as Fig. 3 but with $I=1\times10^{12}$ W/cm^2 (0.005 34 a.u.) and $t=15T$.

We have a keen interest in this case, since experiments using a yttrium aluminum garnet laser with a frequency of 0.043 a.u. (1.17 eV) at intensities approaching 10^{12} W/cm^2 could reach the intense-field regime [1]. We begin our discussion by applying the technique to the weak-field limit. In this case, the rate we extract from our TD evolution should agree with the result of FO perturbation theory. We consider a case at the above frequency ($T=3.53$ fs) and an intensity of 5×10^{10} W/cm^2 ($E_0=0.001\,19$ a.u.), which yields a ratio of the binding to quiver energies of about 140. We choose a K-space mesh ($N_K=70$) divided into seven zones as (5,23,10,10,10,6,6/0,0.10,0.20,0.37,0.50,1.0,3.0,8.0). For the angular variable θ, we select a single zone with ten points. This particular choice yields a matrix of order 700 to be propagated in time at a step of $\Delta t=0.02$ a.u. In Fig 1, we present the effective rate $W(t)$ as a function of time over 20 periods of the radiation field. After an initial transitory phase, the function begins to oscillate about a constant value (1.50×10^{-4} a.u. or 6.2×10^{12} s^{-1}). We find excellent agreement between this value and that calculated from the FO perturbation theory (1.40×10^{-4} a.u.), indicating the efficacy of the method. We also obtain a single EPD peak at an electron energy of 0.0308 Ry, a value very close to the simple conservation of energy condition ($\omega-\epsilon_b$). The p-wave component dominates the electron distribution as predicted by the dipole selection rules. We now turn our attention to the realm of more intense fields.

We consider first a case with the previous frequency and an intensity of 5×10^{11} W/cm^2 (0.003 78 a.u.). We choose a K-space mesh ($N_K=100$) divided into eight zones as (5,25,8,25,7,10,10,5,5/0,0.13,0.18,0.31,0.34, 0.42,0.46,1.0,3.0,8.0) and N_θ to be 10 in order to optimize the mesh to display the EPD structure. This choice leads to the propagation of a matrix of order 1000 by a temporal step of 0.02 a.u. We also tested the convergence by using product mesh sizes of the order of 400 to 1100. In Fig. 2, we display the effective rate $W(t)$ as a function of time. We observe that this quantity oscillates about a constant value, thus giving meaning to the definition of a single period-averaged detachment rate W_a of 1.3×10^{-3} a.u. or 5.37×10^{13} s^{-1}. The detachment probability reaches about 0.5 at the end of ten cycles. In Fig. 3, we present the electron distribution $P_m(K|t)$ summed up to $l=7$ as a function of the wave number K after ten cycles of the field. We note the appearance of several EDP peaks, although the higher ones are rather weak. Their positions fall very close to those predicted by the simple

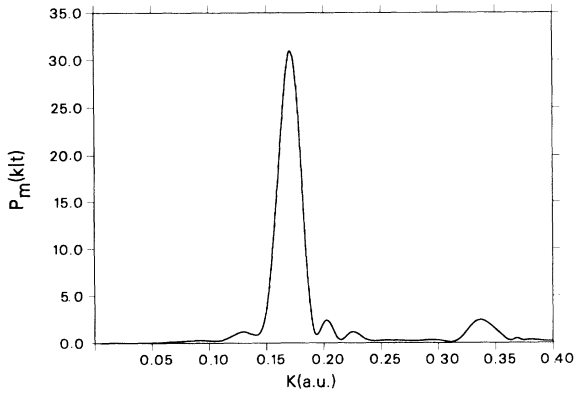

FIG. 3. Electron distribution function $P_m(K|t)$ for $m=0$ as a function of K for $\omega=0.043$ hartree, $I=5\times10^{11}$ W/cm^2, and $t=10T$ with $T=3.53$ fs.

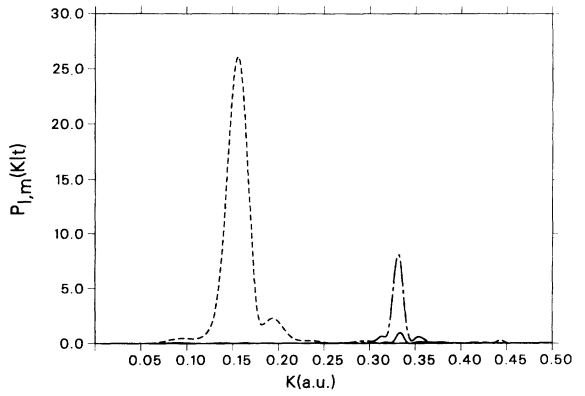

FIG. 5. Electron distribution function $P_{l,m}(K|t)$ for $m=0$ as a function of K and partial wave l for the case described in Fig. 4. The curves are labeled as follows: solid line, $l=0$, dashed line, $l=1$; and chain-dashed lines $l=2$ (d wave).

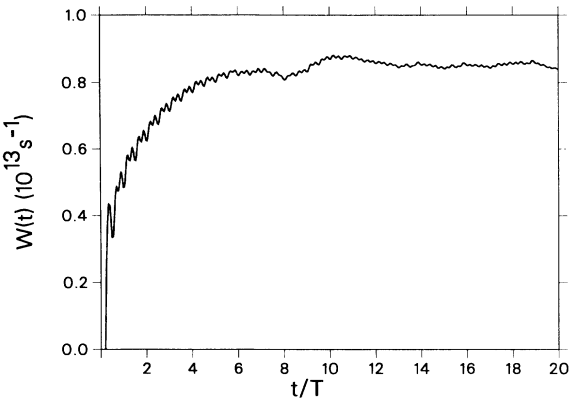

FIG. 6. Effective detachment rate $W(t)$ as a function of time for $\omega=0.018$ hartree (0.49 eV) and an intensity of $I=2.5\times10^{11}$ W/cm^2 (0.002 673 a.u.).

formula (a.u.)

$$E_n=n\omega-\varepsilon_b-E_j\ , \tag{17}$$

where E_j is the quiver energy $E_0^2/(4\omega^2)$ and $K_n=(2E_n)^{1/2}$. Since plots with respect to K give a better display for the EPD peaks, we shall use this format throughout. However, the laser frequency ω still dictates the peak separation, as clearly indicated by Eq. (17), and plots with respect to energy, K^2. The lowest EPD peak is dominated by a p-wave ($l=1$) contribution, while the second peak is a combination of s and d waves. This particular association would be expected from perturbation theory for excitation by one and two photons, respectively.

A more interesting case arises at twice the previous intensity 1×10^{12} W/cm^2 (0.005 34 a.u.). In Fig. 4, we give the electron-energy distribution at $t=15T$, which now shows evidence of three EPD peaks. The mesh and propagation parameters were similar to the preceding example. The system becomes almost totally detached by ten cycles, and the ratio of the height of the first to the second EDP peak remains practically constant at a factor of 2.90. In Fig. 5, we display the partial-wave components of the electron distribution as a function of energy. As in the weaker-field case, the lowest peak is basically p wave and the second peak a mixture of s and d waves, with the d wave giving a larger contribution. The position of the peaks corresponds to Eq. (17) with very little evidence of any additional shift, although the curves do not have the detail to yield precise values. Finally, we present a summary of the rates as a function of intensity in Table I. These results tend to confirm that an experiment with these parameters might glimpse the EPD structure of this simple system.

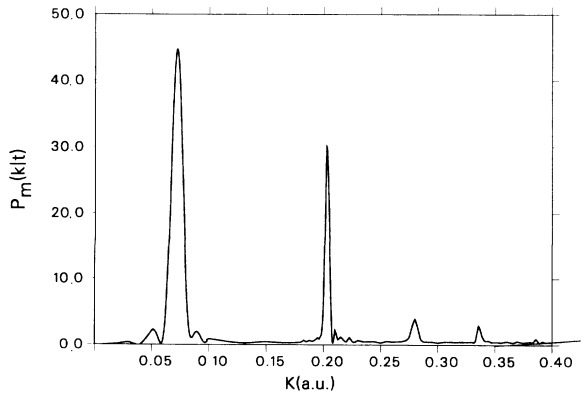

FIG. 7. Electron distribution function $P_m(K|t)$ for $m=0$ as a function of K for the case described in Fig. 6 at $t=20T$.

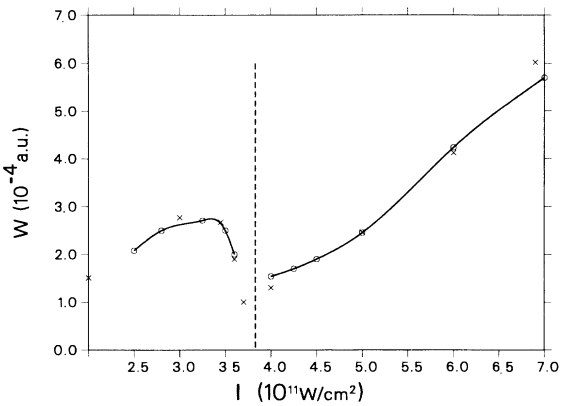

FIG. 8. Period-averaged rate W_a as a function of intensity I for $\omega=0.018$ hartree near the two- to three-photon threshold. Nomenclature: line and circles, present calculations; crosses, Ref. [10]; and vertical dashed line, threshold.

B. Multiphoton detachment

With the ability to tune the laser frequency by means of a relativistic beam [1,2], we can hope to explore other intense-field regimes. We consider a two-photon process with a laser frequency of 0.018 a.u. (0.49 eV, $T=8.44$ fs). We have employed a K-space mesh ($N_K=130$) of the form (5,30,5,20,20,25,10,10,5/0,0.05,0.10,0.18,0.23,0.33, 0.4,0.8,3.0,8.0) and $N_\theta=10$. In Fig. 6, we examine a representative case for the effective rate at an intensity of 2.5×10^{11} W/cm^2 or 0.002 673 a.u. of field strength. We observe the now familiar pattern of an oscillating function about a constant value giving rise to an unambiguous definition of a period-averaged rate $W_a=2.08\times10^{-4}$ a.u. or 8.60×10^{12} s^{-1}. We display the rich EPD spectrum in

TABLE I. Time-averaged ratees W_a for the electron detachment of H^- as a function of intensity for two laser frequencies. Numbers in square brackets give power of 10.

$\hbar\omega=1.17$ eV (0.043 a.u.)		$\hbar\omega=0.49$ eV (0.018 a.u.)	
I (W/cm^2)	W_a (s^{-1})	I (10^{11} W/cm^1)	W_a (s^{-1})
5.0[+10]	6.2[+12]	2.50	8.6[+12]
1.0[+11]	1.2[+13]	2.80	1.0[+13]
2.0[+11]	2.3[+13]	3.25	1.1[+13]
5.0[+11]	5.4[+13]	3.50	1.0[+13]
1.0[+12]	8.3[+13]	4.00	6.4[+12]
2.0[+12]	1.2[+14]	5.00	7.9[+12]
		6.00	1.7[+13]
		7.00	2.4[+13]

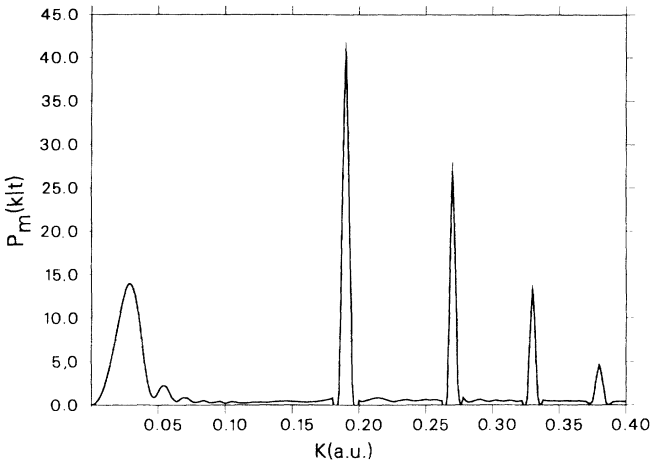

FIG. 9. Same as Fig. 7 but with $I=3.5\times10^{11}$ W/cm^2 (0.003 162 a.u.) at $t=20T$.

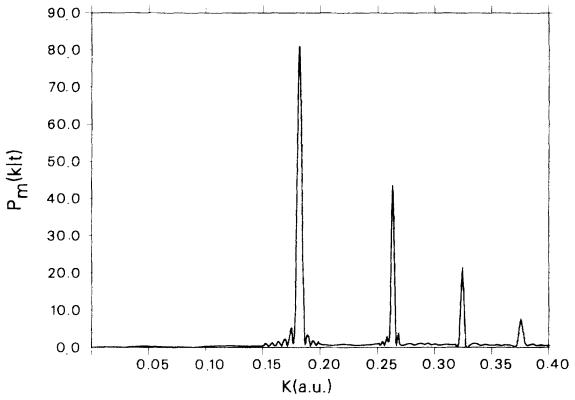

FIG. 10. Same as Fig. 7 but with $I=4.25\times10^{11}$ W/cm^2 (0.003 485 a.u.) at $t=20T$.

Fig. 7, demonstrating the well-established phenomenon that higher-order photon processes exhibit intense-field effects at lower intensities.

Scrutiny of Eq. (17) suggests an interesting scenario. For fixed frequency ω and number of photons n, we can adjust the laser field E_0 such that the electron energy is zero. For higher intensities, the electron detachment energy becomes negative, indicating that an additional photon must be absorbed to raise the electron into the continuum. Therefore, this critical-field demarcates the threshold between n and $n+1$ photon absorption. In order to explore this interesting region, we concentrate on the two- to three-photon threshold, which occurs at an intensity of 3.83×10^{11} W/cm^2 for a frequency of 0.018 a.u. In Fig. 8 and Table I, we display the rate W_a as a function of intensity. Circles mark the actual calculated points, while the solid line serves as a visual aid; the vertical dashed line gives the predicted threshold. We also show a comparison with the results of a Floquet calculation [10] for the same model potential. The agreement is very good, considering the different formulations involved. In this particular case, the Keldysh-style techniques lie within about 30% of the Floquet results [10]. We notice that the rate decreases as a function of intensity near the threshold. We have left a gap in our curve very close to the threshold since we find that a single rate cannot describe the detachment process in this region. We in effect have a competition between different mechanisms that we cannot cleanly resolve during the length of our longest temporal propagation ($30T$). Once we pass threshold, we can again uniquely define a rate, which then increases until reaching the next threshold where similar behavior ensues.

We can understand this behavior in terms of a basic threshold effect. In the intense-field regime, the photon absorption must have sufficient energy not only to break the atomic bound (ε_b), but also to supply the freed electron with its proper motion within the laser field (E_j). For a fixed frequency and increasing intensity, we eventually encounter a situation in which the energy remaining to the electron after detachment is insufficient to initiate the quiver motion. In this case, another photon is needed to promote the electron into the continuum. In order to examine the behavior near the threshold in more detail, we present in Figs. 9 and 10 the electron distribution $P_m(K|t)$ for intensities of 3.5×10^{11} and 4.25×10^{11} W/cm^2, respectively. At an intensity well below the threshold (2.5×10^{11} W/cm^2), we observe a rich EPD spectrum with a dominant initial peak as depicted in Fig. 7. Just below the threshold, we note the suppression of the first peak. For the higher intensity, this peak has entirely disappeared. Such behavior has been well documented in both 1D [18–24] and 3D [18] models. We do not find any evidence of a trapping near the nucleus of the wave function, as may be seen in more intense fields. We have verified this behavior through extensive one-dimensional calculations in which the same basic phenomena occurs.

In this paper, we have explored a variety of processes associated with the photodetachment of the hydrogen negative ion in the intense-field regime. We observe such effects as excess-photon detachment and suppression of the detachment rate near thresholds. We have employed a fully time-dependent treatment of the Schrödinger equation in momentum space to investigate these regimes.

ACKNOWLEDGMENTS

We wish to thank Professor R. Shakeshaft for sending us the numerical values of the detachment rate described in Ref. [10]. We also acknowledge useful discussions with Dr. K. Kulander, Dr. G. Csanak, Dr. H. Bryant, and Dr. K. LaGattuta. This work was performed under the auspices of the U.S. Department of Energy through the Theoretical Division at the Los Alamos National Laboratory.

[1] C. Y. Tang, P. G. Harris, A. H. Mohagheghi, H. C. Bryant, C. R. Quick, J. B. Donahue, R. A. Reeder, S. Cohen, W. W. Smith, and J. E. Stewart, Phys. Rev. A **39**, 6068 (1989); C. T. Tang, H. C. Bryant, P. G. Harris, A. H. Mohagheghi, R. A. Reeder, H. Sharifian, H. Tootoonchi, C. R. Quick, J. B. Donahue, S. Cohen, and W. W. Smith, Phys. Rev. Lett. **66**, 3124 (1991).

[2] P. G. Harris, H. C. Bryant, A. H. Mohagheghi, R. A. Reeder, C. T. Tang, J. B. Donahue, and C. R. Quick, Phys. Rev. A **42**, 6443 (1990).

[3] C. Blondel, M. Crance, C. Delsart, and A. Giraud, J. Phys. B **24**, 3575 (1991).

[4] M. D. Davidson, H. G. Muller, and H. B. van Linden van-den Heuvell, Phys. Rev. Lett. **67**, 1712 (1991).

[5] H. Stapelfelt, P. Balling, C. Brink, and H. K. Haugen, Phys. Rev. Lett. **67**, 1731 (1991).

[6] L. V. Keldysh, Zh. Eksp. Teor. Fiz. **47**, 1945 (1964) [Sov. Phys. JETP **20**, 1309 (1965)].

[7] F. H. M. Faisal, J. Phys. B **6**, L89 (1973).

[8] H. R. Reiss, Phys. Rev. A **22**, 1786 (1980); **42**, 1476 (1990).

[9] R. Shakeshaft and X. Tang, Phys. Rev. A **36**, 3193 (1987).

[10] M. Dörr, R. M. Potvliege, and R. Shakeshaft, Phys. Rev. A **42**, 4138 (1990).

[11] R. M. Potvliege and R. Shakeshaft, Phys. Rev. A **38**, 4597 (1988).

[12] M. Crance, J. Phys. B **20**, 6553 (1987); J. Phys. B **21**, 3559 (1988).

[13] D.-S. Guo, T. Åberg, and B. Craseman, Phys. Rev. A **40**, 4997 (1989).

[14] X. Mu, J. Ruschienski, and B. Craseman, Phys. Rev. A **42**, 2949 (1990).

[15] X. Mu, Phys. Rev. A **42**, 2944 (1990).

[16] W. Becker, J. K. McIver, and M. Confer, Phys. Rev. A **40**, 6904 (1989).

[17] T. Merouris and C. A. Nicolaides, J. Phys. B **23**, 2037 (1990); **24**, L57 (1991).

[18] L. A. Collins and A. L. Merts, J. Opt. Soc. Am. B **7**, 647 (1990); Phys. Rev. A **40**, 4127 (1989); **37**, 2415 (1988).

[19] Multielectron Excitations in Atoms, J. Opt. Soc. Am. **4** (5), 705 (1987) (entire issue), edited by W. E. Cooke and T. J. McIlrath.

[20] Theory of High-Order Processes in Atoms in Laser Fields, J. Opt. Soc. Am. **7** (4), 403 (1990) (entire issue), edited by K. Kulander and A. L'Hullier.

[21] J. H. Eberly and J. Javananiner, Eur. J. Phys. **9**, 265 (1988).

[22] P. Milonni, in *Atoms in Strong Fields,* edited by C. Nicolaides, C. W. Clark, and M. H. Nayfeh (Plenum, New York, 1990).

[23] *Atoms in Unusual Situations,* Vol. 143 of NATO Advanced Study Institute, Series B: Physics, edited by J. P. Birandd (Plenum, New York, 1986).

[24] K. C. Kulander, K. J. Schafer, and J. L. Krause, Adv. At. Mol. Opt. Phys. (to be published).

[25] Time Dependent Methods for Quantum Dynamics, Comput. Phys. Commun. **63** (1991) (entire issue), edited by K. C. Kulander.

[26] C. Leforestier, R. H. Bissling, C. Cerjan, M. D. Feit, R. Friesner, A. Guldberg, A. Hammerich, G. Jolicard, W. Karrlein, H.-D. Meyer, N. Lipkin, O. Roncero, and R. Kosloff, J. Comput. Phys. **94**, 59 (1991).

[27] R. B. Gerber, R. Kosloff, and M. Berman, Comput. Phys. Rep. **5**, 61 (1986).

[28] D. M. Volkov, Z. Phys. **94**, 250 (1935).

[29] C. W. Gear, *Numerical Initial Value Problems in Ordinary Differential Equations* (Prentice-Hall, Englewood Cliffs, NJ, 1985).

[30] T. J. Park and J. C. Light, J. Chem. Phys. **85**, 5870 (1986).

[31] L. A. Collins and G. Csanak, Phys. Rev. A **44**, 5343 (1991).